Proceedings of ASME Turbo Expo 2011
GT2011
June 6-10, 2011, Vancouver, British Columbia, Canada

GT2011-45143

NONLINEAR FAULT DIAGNOSIS OF JET ENGINES BY USING A MULTIPLE MODEL-BASED APPROACH

E. Naderi*, N. Meskin†, and K. Khorasani ‡

ABSTRACT

In this paper, a nonlinear fault detection and isolation (FDI) scheme that is based on the concept of multiple model (MM) approach is proposed for jet engines. A modular and a hierarchical architecture is proposed which enables the detection and isolation of both single as well as concurrent permanent faults in the engine. A set of nonlinear models of the jet engine in which compressor and turbine maps are used for performance calculations corresponding to various operating modes of the engine (namely, healthy and different fault modes) is obtained. Using the multiple model approach the probabilities corresponding to the engine modes of operation are first generated. The current operating mode of the system is then detected based on evaluating the maximum probability criteria. The performance of our proposed multiple model FDI scheme is evaluated by implementing both the Extended Kalman Filter (EKF) and the Unscented Kalman Filter (UKF). Simulation results presented demonstrate the effectiveness of our proposed multiple model FDI algorithm for both structural and actuator faults in the jet engine.

Nomenclature

Subscripts

amb	Ambient
C	Compressor
CC	Combustion chamber
d	Intake
f	Fuel
M	Mixer
mech	Mechanical
n	Nozzle
T	Turbine

Variables

β	Bypass ratio
$\dot{m}$	Mass flow rate, $\frac{Kg}{s}$
η	Efficiency
γ	Heat capacity ratio
c_p	Specific heat at constant pressure, $\frac{J}{Kg.K}$
c_v	Specific heat at constant volume, $\frac{J}{Kg.K}$
H_u	Fuel specific heat, $\frac{J}{Kg}$
J	Rotor moment of inertia, $Kg.m^2$
M	Mach
N	Rotational Speed, RPM
P	Pressure, Pascal
P_0	Pressure at sea level at Standard Day
R	Gas Constant, $\frac{J}{Kg.K}$
T	Temperature, K
T_0	Temperature at sea level at Standard Day
V	Volume, m^3

1 Introduction

The increasing complexity of aerospace vehicles and their systems such as engines, and the cost reduction measures that have affected aircraft and engine manufacturers and maintenance operators are increasingly driving the need for more intelligence

*E. Naderi and K. Khorasani are with the Department of Electrical and Computer Engineering, Concordia University, Montreal, Quebec, H3G 1M8 Canada (Contact email:kash@ece.concordia.ca).

†N. Meskin was with the Department of Electrical and Computer Engineering, Concordia University, Montreal, Quebec, Canada. He is now with the Department of Electrical Engineering, Qatar University, Doha, Qatar.

‡This research is supported in part by a grant from the Natural Sciences and Engineering Research Council of Canada (NSERC) under the industrial Collaborative Research and Development (CRD) partnership program.

and autonomous capabilities and functionalities for diagnosis, prognosis, and health management (DPHM) of these safety critical systems. The objective of an aircraft engine DPHM system is to provide monitoring, predictive trend analysis, detection and diagnosis of faults in the complex engine system. Increased design complexity, strict security and safety requirements, and the need for reduction of the life cycle cost make it necessary to move forward from conventional simple statistical trend analysis and monitoring practices towards an integrated DPHM system that can both autonomously and in real-time interact with human experts to address the above-mentioned issues.

The functionality of a health management system (DPHM) depends to a large extent on the reliability of its corresponding fault detection and isolation (FDI) scheme, issues that have received considerable attraction in the literature. Some excellent surveys ([1] and [2]) have been published that summerize the extensive literature on FDI. One of the FDI approaches that have been proposed , and applied to a few areas is the Multiple-Model Based approach ([3], [4], [5], [6] and [7]). The term "Multiple-Model" covers a wide range of approaches in which the common goal is to propose an architecture (or hierarchy) for a bank of estimators for isolation and identification of faults. The differences arise due to application domain, configurations used and the estimator types invoked.

The FDI problem for linear systems has received considerable attention in the literature, although many industrial applications are governed by nonlinear characteristics which do necessitate the development of nonlinear FDI schemes. Certain approaches that are developed for FDI of linear systems can be extended to nonlinear systems. Among the natural extensions of linear approaches to the nonlinear schemes is to use observer-based schemes given that nonlinear observer design strategies have been established in the literature. A survey of such approaches can be found in [8]. Recent advanced techniques based on geometric approach ([9]) and adaptive estimation approach ([10]) have also been investigated in the literature that provide alternative treatments toward the nonlinear FDI problem. However, the problem of fault diagnosis for nonlinear systems is still an open area of research since the above proposed approaches impose certian restrictions on the nonlinearities of the system to be diagnosed.

Since the early interest and research on FDI, jet engines have been one of the application fields that has been a popular domain for verification, validation, and demonstration of novel methodologies. For example, Patton *et al* have implemented their robust FDI method on jet engines ([11], [12]). The main theme of research in jet engine FDI is based on Gas Path Analysis (GPA) in which by measurement and estimation of lumped parameters of the system such as temperature and pressure at each stage, one attempts to isolate and identify actuator, sensor, or component faults. This approach has mainly been developed by Urban ([13]) and Volponi ([14]). Based on the GPA, various FDI algorithms have been developed with the application of a bank of estimators as proposed by Merrill *et al* ([15]). A multiple model approach that has utilized linear Kalman filters as estimators is also investigated by Kobayashi *et al* ([16]). The application of both linear and nonlinear Kalman filters is a common methodoly in jet engine fault diagnosis as reported by Simon ([17]) which has compared the performance of Linear Kalman Filter (LKF), Extended Kalman Filter (EKF), and Unscented Kalman Filter (UKF) for this application. Simon ([17]) has concluded that both the EKF and the UKF outperforms the LKF, however, there was no considerable difference reported between the performance of the EKF and the UKF. In this work we have shown that through the utilization of our proposed multiple model framework the UKF filters do indeed outperform the EKF filters as discussed below.

In this paper, a multiple model (MM)-based scheme that employs nonlinear Kalman filters as state estimators (detection filters) is developed and implemented for the first time in the literature for fault diagnosis of jet engines. This is a natural extension of our previous work ([18]) in which we have proposed a MM-based approach that employed LKF as state estimators (detection filters). This is partially motivated by the limitations of the MM-based approach that uses LKF in its structure that makes it incapable of fully coping with the variations in the ambient conditions and power settings.

Our proposed MM-based fault diagnosis approach assumes that the dynamics of the engine is adequately represented by a nonlinear model that is parameterized by a fault vector. It is further assumed that the fault vector can take only M discrete values corresponding to the normal and various failure modes in the engine. The nonlinear model corresponding to each fault vector is obtained from the fully nonlinear model of the system, and a bank of nonlinear Kalman filters is then designed where each nonlinear Kalman filter corresponds to and is associated with a specific value of the fault vector. The conditional probabilities of each discrete parameter value being the correct one, given the measurement history, are calculated iteratively by using the Baye's law. The current operating mode of the engine is then determined based on the maximum probability criteria. Moreover, a hierarchical approach is proposed where multiple levels of the detection filters are designed that according to the current engine status and operating mode (that is healthy or faulty), only an appropriate set of the bank of filters becomes and is active at any given time. This hierarchical architecture enables the detection and isolation of the engine concurrent faults without imposing any additional computational load on the FDI scheme as compared to the single fault detection and isolation case.

Simulation results presented for a single spool jet engine demonstrate the effectiveness and capabilities of our proposed fault diagnosis framework and algorithm. In order to simulate the transient response of the jet engine, a modular SIMULINK model of the nonlinear dynamics of the jet engine is devel-

oped. Moreover, for accurate calculations of the jet engine performance, the engine components are modeled by corresponding performance maps [19, 20]. These maps are adopted from a commercial software GSP [21]. We have investigated the performance of both the Extended Kalman Filter (EKF) and the Unscented Kalman Filter (UKF) as state estimators (detection filters) in our proposed MM-based architecture. Simulation results convincingly verify that indeed considerable improvements are obtained in the performance of the UKF over that of the EKF schemes in terms of the fault detection time and functionality with different sets of measurements. Moreover, the UKF FDI scheme is significantly more robust to the sensor noise.

The remainder of this paper is organized as follows. In Section 2, a brief overview of the multiple model (MM) approach is presented. A nonlinear mathematical model of a jet engine that is considered for design and testing of our proposed fault detection and isolation (FDI) multiple model approach is developed in Section 3. In Section 4, the MM-based FDI algorithm is formally proposed and developed for a jet engine. In Section 5, simulation results corresponding to different fault scenarios in the jet engine are presented, and comparisons between the EKF and the UKF schemes in terms of their sensitivity to external noise levels and availability of the measurements are conducted. Conclusions and future work are presented in Section 6.

2 MM-based FDI Algorithm

In this section, a brief overview of the multiple model (MM)-based fault detection and isolation (FDI) scheme is presented [3]. Let $\mathbf{a}$ denote the vector of fault parameters in a given dynamical system where it can take on only one of the M representative values $\mathbf{a}_i, i = 1,...,M$. The model corresponding to $\mathbf{a}_i$ is described by the following nonlinear discrete-time system

$$\begin{aligned} x(k+1) &= f_i(x(k),u(k)) + \xi_i(k) \\ z(k) &= h_i(x(k)) + \eta_i(k) \end{aligned} \tag{1}$$

where $x(k)$ is the state of the system, $z(k)$ is the measurement vector, and $u(k)$ is the control input vector. The fault parameter $\mathbf{a}_i$ may correspond to the actuator, the sensor or the structural faults in the system. For instance, in the single-spool jet engine model that is considered in this paper we have the following specific definitions, namely $x = [P_{CC}, N, T_{CC}, P_T]^T$, $z = [T_C, P_C, N, T_T, P_T]^T$, and u is the power level angle (PLA) (refer to the nomenclature section for the physical meaning and definitions of these variables). The process and the measurement noise vectors ξ_i and η_i are mutually independent white Gaussian noise of zero mean and covariance Q_i and R_i, respectively.

Remark 1. *For sake of illustration and as shown subsequently in Section 4, for the jet engine considered in this work we take $M = 6$, where the parameter a_1 corresponds to the healthy mode of the engine, the parameters $a_2,...,a_5$ correspond to the common jet engine component faults, and the parameter a_6 denotes the fuel flow valve fault.*

The Prediction Step
$\hat{x}_i^-(k) = f_i(\hat{x}_i(k-1), u_i(k-1))$
$P_i^-(k) = A_i(k)P_i(k-1)A_i^T(k) + Q_i$
The Update Step
$v_i(k) = z_i(k) - h_i(\hat{x}_i^-(k))$
$S_i(k) = C_i(k)P_i^-(k)C_i^T(k) + R_i$
$K_i(k) = P_i^-(k)C_i^T(k)S_i^{-1}(k)$
$\hat{x}_i(k) = \hat{x}_i^-(k) + K_i(k)[y_i(k) - h_i(\hat{x}_i^-(k))]$
$P_i(k) = (I - K_i(k)C_i(k))P_i^-(k)$
Notation
$A_i(k) = \frac{\partial f_i}{\partial x}\|_{\hat{x}_i(k-1), u_i(k-1)}$
$C_i(k) = \frac{\partial h_i}{\partial x}\|_{\hat{x}_i^-(k)}$

Table 1. The Extended Kalman Filter Algorithm

Let the hypothesis conditional probability $p_i(k)$ be defined as the probability that $\mathbf{a}$ assumes the value $\mathbf{a}_i$ (for $i = 1,...,M$), conditioned on the observed measurement history up to time k, that is

$$p_i(k) = Pr[\mathbf{a} = \mathbf{a}_i | \mathscr{Z}(k) = \mathscr{Z}_k] \tag{2}$$

where the measurement history random vector $\mathscr{Z}(k)$ is made up of the partitions $z(1),...,z(k)$ that represent the available measurements up to the kth sample time and similarly, the realization $\mathscr{Z}_k$ of the measurement history vector has partitions $z_1,...,z_k$ [3]. It can be shown that $p_i(k)$ can be evaluated recursively for all i via the iteration

$$p_i(k) = \frac{F_{z(k)|\mathbf{a},\mathscr{Z}(k-1)}(z_i|\mathbf{a}_i, \mathscr{Z}_{k-1}) p_i(k-1)}{\sum_{j=1}^{M} F_{z(k)|\mathbf{a},\mathscr{Z}(k-1)}(z_i|\mathbf{a}_j, \mathscr{Z}_{k-1}) p_j(k-1)} \tag{3}$$

in terms of the previous values of $p_1(k-1),...,p_M(k-1)$, and conditional probability densities for the current measurement $z(k)$ (denoted by $F_{z(k)|\mathbf{a},\mathscr{Z}(k-1)}(z_i|\mathbf{a}_i, \mathscr{Z}_{k-1})$).

The MM-based FDI scheme is now composed of a bank of M individual and separate nonlinear Kalman filters, each based on a particular value of $\mathbf{a}_i$, $i = 1,...,M$. The innovation vector $v_i(k)$ is used to compute $p_1(k),...,p_M(k)$ via equation (3) with a Gaussian density function that is given by

$$F_{z(k)|m,\mathscr{Z}(k-1)}(z_i|\mathbf{a}_i, \mathscr{Z}_{k-1}) = \zeta_i(k) e^{-(1/2)v_i'(k)S_i^{-1}(k)v_i(k)} \tag{4}$$

where $\zeta_i(k) = \frac{1}{(2\pi)^{m/2}|S_i(k)|^{1/2}}$ and m is the measurement dimension. The innovation $v_i(k)$ and the innovation covariance matrix

The Prediction Step
Augmentation
$x_i^a(k-1) = \left[\hat{x}_i^T(k-1)\ E[\xi_i^T(k)]\right]^T$
$P_i^a(k-1) = \begin{bmatrix} P_i(k-1) & 0 \\ 0 & Q_i \end{bmatrix}$
Sigma Points
$\chi_i^0(k-1) = x_i^a(k-1)$
$\chi_i^j(k-1) = x_i^a(k-1) + \left(\sqrt{(L+\lambda)P_i^a(k-1)}\right)_j \quad j = 1...L$
$\chi_i^j(k-1) = x_i^a(k-1) - \left(\sqrt{(L+\lambda)P_i^a(k-1)}\right)_j \quad j = L+1...2L$
Time Update
$\chi_i^{j^-}(k) = f(\chi_i^j(k-1), u_i(k-1))$
$\hat{x}_i^-(k) = \sum_{j=0}^{2L} W_m^j \chi_i^{j^-}(k)$
$P_i^-(k) = \sum_{j=0}^{2L} W_c^j \left[\chi_i^{j^-}(k) - \hat{x}_i^-(k)\right]\left[\chi_i^{j^-}(k) - \hat{x}_i^-(k)\right]^T$
The Update Step
Augmentation
$x_i^{-a}(k) = \left[\hat{x}_i^{-T}(k)\ E[\eta_i^T(k)]\right]^T$
$P_i^{-a}(k) = \begin{bmatrix} P_i^-(k) & 0 \\ 0 & R_i \end{bmatrix}$
Sigma Points
$\chi_i^{0^-}(k) = x_i^{-a}(k)$
$\chi_i^{j^-}(k) = x_i^{-a}(k + \left(\sqrt{(L+\lambda)P_i^-(k)}\right)_j \quad j = 1...L$
$\chi_i^{i^-}(k) = x_i^{-a}(k - \left(\sqrt{(L+\lambda)P_i^-(k)}\right)_j \quad j = L+1...2L$
Measurement Update
$\mathcal{Y}_i^j(k) = h(\chi_i^{j^-}) \ j = 1...2L$
$\hat{y}_i(k) = \sum_{j=0}^{2L} W_m^j \mathcal{Y}_i^j(k)$
$v_i(k) = z_i(k) - \hat{y}_i(k)$
$S_i(k) \equiv P_{\hat{y}\hat{y}_i}(k) = \sum_{j=0}^{2L} W_c^j \left[\mathcal{Y}_i^j(k) - \hat{y}_i(k)\right]\left[\mathcal{Y}_i^j(k) - \hat{y}_i(k)\right]^T$
$P_{\hat{x}\hat{y}_i}(k) = \sum_{j=0}^{2L} W_c^j \left[\chi_i^{j^-}(k) - \hat{x}_i^-(k)\right]\left[\mathcal{Y}_i^j(k) - \hat{y}_i(k)\right]^T$
$K_i(k) = P_{\hat{x}\hat{y}_i}(k) P_{\hat{y}\hat{y}_i}^{-1}(k)$
$\hat{x}_i(k) = \hat{x}_i^-(k) + K_i(k)\left[y_i(k) - \hat{y}_i(k)\right]$
$P_i(k) = P_i^-(k) - K_i(k) P_{\hat{y}\hat{y}_i}(k) K_i^T(k)$
Notation and Parametrization
$(\sqrt{A})_j$ denotes the jth row of $\sqrt{A}$
L is the dimension of the augmented state
$W_m^0 = \frac{\lambda}{L+\lambda}$
$W_c^0 = \frac{\lambda}{L+\lambda} + (1 - \alpha^2 + \beta)$
$W_m^j = W_c^j = \frac{1}{2(L+\lambda)}$
$\lambda = \alpha^2(L+\kappa) - L$
$\alpha = 0.001; \kappa = 0; \beta = 2$

Table 2. The Unscented Kalman Filter Algorithm

$S_i(k)$ are computed by using the standard equations of the Extended Kalman Filter (EKF) and the Unscented Kalman Filter (UKF) as given in Tables 1 and 2 ([17], [22]), respectively.

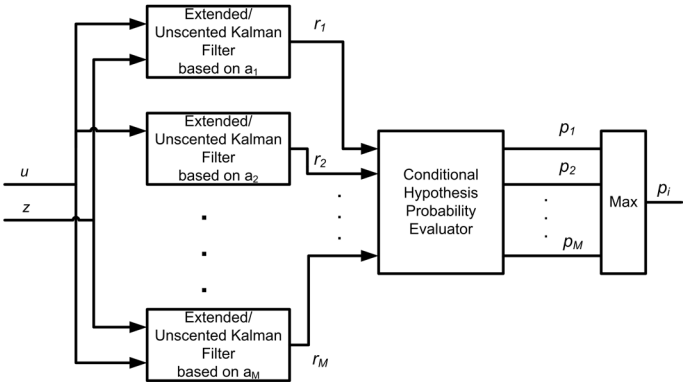

Figure 1. General architecture of our proposed MM-based FDI scheme.

Let us assume that the actual value of the fault parameter $\mathbf{a}$ is given by $\mathbf{a}_i$. Then, it is expected that a mean squared value of the residual generated by the nonlinear Kalman filter based on $\mathbf{a}_i$ is in consonance with the residual covariance matrix $S_i(k)$ over time, while mismatched filters generate larger residuals than those predicted by the their own residual covariance matrices. Hence, the MM-based algorithm will most heavily weight the nonlinear Kalman filter that corresponds to $\mathbf{a}_i$. The problem of fault detection and isolation (FDI), or equivalently the status of the current operating mode of the system at the time instant k can therefore be stated as and simplified to that of evaluating the quantity $\arg\max_i p_i(k)$ for the desired solution. Figure 1 shows the schematic of the general architecture of our proposed MM-based FDI approach.

Remark 2. *It follows from equation* (3) *that if any p_i is ever computed to be zero at any given time k, this probability will be locked to zero for all time there after. In order to prevent this lock out [3], an artificially small lower bound was considered for all p_i's. Moreover, it was shown in [23] that the leading coefficient $\zeta_i(k)$ in* (4) *does not provide any useful information for fault identification and even may cause incorrect fault identification. Therefore, the term $\zeta_i(k)$ is usually removed from the equation* (4)*. It should be noted that since the denominator of* (3) *is the summation of all the numerators, even by removing the term $\zeta_i(k)$, the sum of the computed probabilities remains one.*

3 The Jet Engine Mathematical Model

Based on the available literature on modeling a nonlinear dynamics of a jet engine ([24] and [25]), a SIMULINK model for a single spool engine is first developed. In order to obtain this nonlinear dynamics, rotor and volume dynamics are both considered. Heat transfer dynamics also contributes to this nonlinear behavior particularly when there exist considerable differences between the temperatures of the air stream and the components due to a large power excursion, e.g. during the takeoff or rapid

maneuvers of an agile aircraft ([26]). Nevertheless, the above effect has been neglected since in this paper we are concerned with a commercial single spool jet engine at normal operating conditions. We have used the commercial software GSP 10 ([21]) for the purposes of obtaining the required data such as the compressor map as well as conducting model validation studies. A more detailed description of the model can be found in [24], [25] and [27].

3.1 Governing nonlinear equations of the motion

In this section, a set of nonlinear equations corresponding to a single spool jet engine is provided. In the engine intakes, by assuming adiabatic process, the pressure and the temperature behavior are evaluated. For the compressor, the pressure ratio π_C is calculated from the volume dynamics of the combustion chamber. The rotational speed (N) is obtained from the solution of the energy balance for the spool that is connecting the compressor to the turbine. Once the pressure ratio and the rotational speed are computed, the corrected mass flow and the efficiency behaviors are obtained from the performance map, so that the temperature rise can be obtained. Finally, the pressure ratio of the turbine is obtained from the volume dynamics of the nozzle.

The above process and dynamics can be formally summarized according to the nonlinear set of governing equations of motion for a single spool jet engine as follows

$$\begin{aligned}
\dot{T}_{CC} &= \frac{1}{c_v m_{CC}}[(c_p T_C \dot{m}_C + \eta_{CC} H_u \dot{m}_f - c_p T_{CC} \dot{m}_T) - \\
&\quad c_v T_{CC}(\dot{m}_C + \dot{m}_f - \dot{m}_T)] \\
\dot{N} &= \frac{\eta_{mech} \dot{m}_T c_p (T_{CC} - T_T) - \dot{m}_C c_p (T_C - T_d)}{JN(\frac{\pi}{30})^2} \\
\dot{P}_T &= \frac{RT_M}{V_M}(\dot{m}_T + \frac{\beta}{1+\beta}\dot{m}_C - \dot{m}_n) \\
\dot{P}_{CC} &= \frac{P_{CC}}{T_{CC}}\dot{T}_{CC} + \frac{\gamma R T_{CC}}{V_{CC}}(\dot{m}_C + \dot{m}_f - \dot{m}_T)
\end{aligned} \tag{5}$$

where η_{mech} denotes the mechanical efficiency and J denotes the inertia of the shaft connecting the compressor to the turbine. Furthermore, using [24] the following dynamics for the fuel mass flow rate are considered

$$\tau \frac{d\dot{m}_f}{dt} + \dot{m}_f = G u_{fd} \tag{6}$$

where τ is the time constant, G is the gain associated with fuel valve and u_{fd} denotes the fuel demand which is computed by using a feedback from the rotational speed as described in [24].

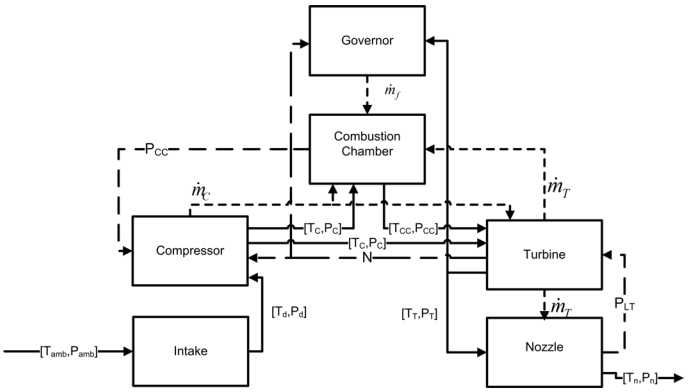

Figure 2. Information flow diagram in a modular modeling of the jet engine dynamics.

A modular Simulink model is developed to simulate the above jet engine nonlinear dynamics as described by equations (5) and (6). Figure 2 shows the information flow process in our Simulink model of the engine.

3.2 Validation of the mathematical model

Figure 3 shows the series of steady states that are obtained from our nonlinear model and the GSP [21] at PLAs ranging from 0.4 to 1. At each point, the initial condition of the PLA is set equal to 0.3 followed by a transient to reach to the steady state corresponding to the desired PLA. Since the steady state corresponding to each PLA is independent of the path taken during the transient (unless the compressor surges), it provides a suitable basis for comparison.

As can be observed from Figure 3 the responses corresponding to our model and the GSP match each other within an acceptable error tolerance(below 5%). The difference between the two representations is manifested in terms of the complexity of the mathematical model used where our form is simpler as compared to the the more complicated representation of the GSP ([21]). Moreover, transient responses that are obtained from our model for different scenarios are in good agreement with the GSP results. For instance, Figure 4 shows a comparison of the transient responses of our model and the GSP to an input profile. The above observations do indeed demonstrate our model is valid for simulation of the nonlinear dynamics of a jet engine.

4 MM-based Fault Diagnosis Design

In this section, a fault detection and isolation (FDI) strategy for a single spool jet engine that is based on the MM-based approach is developed. Towards this end, first the nonlinear Kalman filters corresponding to each operating mode (healthy and faulty) is derived. The MM-based nonlinear filters are then

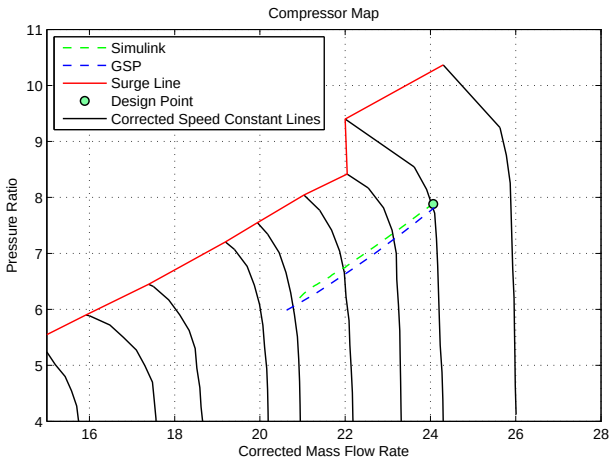

Figure 3. Steady state series at PLAs ranging from 0.4 to 1 on the compressor performance map.

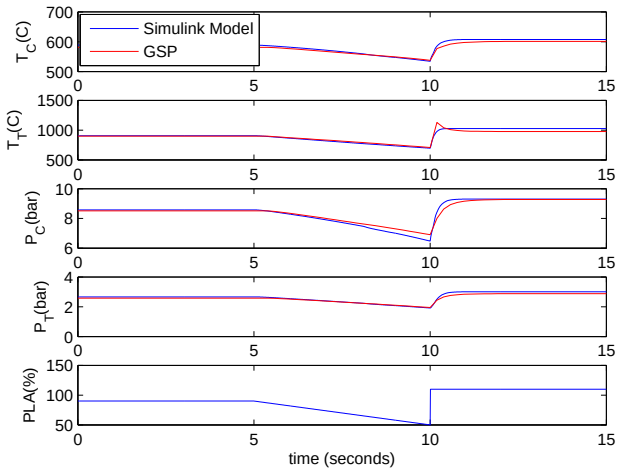

Figure 4. Transient responses of our Simulink Model and the GSP [21] to an input profile.

designed according to the procedure that is described in Section 2. As pointed out after equation (1), the output measurements, z, or the available sensors are taken as the pressure and the temperature after the compressor (P_C and T_C), the pressure and the temperature after the turbine (P_T and T_T), and the rotational speed (N).

4.1 Fault Modeling and Detection Filter Design

In this paper, both component anomalies as well as an actuator anomaly are considered as sources of jet engine faults. Common component faults [14] are modeled as changes in the component efficiency and flow capacity. Four component faults are investigated in this work as shown in Table 3. Moreover, a fault in the fuel valve is considered as an actuator fault. Hence,

Component Fault	Description	Mode Label
ΔFC_C	Decrease in the compressor flow capacity	P2
$\Delta\eta_C$	Decrease in the compressor efficiency	P3
ΔFC_T	Decrease in the turbine flow capacity	P4
$\Delta\eta_T$	Decrease in the turbine efficiency	P5

Table 3. The definition and description of the considered component faults.

the total number of operating modes is **six** (as stated in Remark 1) where mode #1 (P1) corresponds to the healthy jet engine, modes #2 to #5 (P2 to P5) correspond to the component faults as specified in Table 3, and mode #6 (P6) corresponds to the loss of effectiveness fault in the fuel valve actuator (equation(6)). Faults that are considered here are multiplicative e.g. the fault compressor efficiency is defined as $\Delta\eta_C \times \eta_C$.

Faulty models corresponding to the component faults in Table 3 are obtained by considering a 2% decrease in the efficiency or the flow capacity with respect to the normal (healthy) mode. For instance, for obtaining the nonlinear model associated with the operating mode #2, the compressor efficiency is decreased by 2% [28, 29]. Moreover, the nonlinear model associated with the operating mode #6 (actuator fault mode) is obtained by considering a 5% loss of effectiveness or gain fault in the fuel actuator valve.

In our proposed hierarchical approach, it is assumed that the engine starts from the healthy condition when the "first level" of filters are active and the proposed algorithm observes the engine for occurrence of one of the five faults that are specified above. Normally, when the engine is operating healthy, the mode probability corresponding to the first mode (#1) is maximum. Once a fault has occurred, the mode probability corresponding to the healthy mode decreases, and the mode probability corresponding to the occurred fault increases until it takes the maximum value among all the modes. The maximum value of the mode probability that is reached by the active mode is 1, and the corresponding probabilities of other modes become 0. Therefore, the fault detection logic is simply a comparison among the mode probabilities by which the corresponding fault is detected and isolated.

For detection and isolation of two concurrent faults in the engine, a hierarchical approach is proposed [3] as illustrated in Table 4. Once the first fault is detected and isolated according to the maximum probability criteria, the FDI algorithm will activate the "second level" of filters (as shown in Table 4) for detection and isolation of the second concurrent fault in the engine. It should be noted that in our proposed hierarchical architecture, it is assumed that faults do not occur simultaneously and there exists at least a non-zero time interval (dwell time) between the occurrence of faults in the engine. In other words, we are considering and allowing the occurrence of concurrent faults. Table

Levels	Operating Modes					
	# 1	# 2	# 3	# 4	# 5	# 6
First	Healthy	P2 (2%)	P3 (2%)	P4 (2%)	P5 (2%)	P6 (2%)
Second	P2	P2 (5%)	P2 P3	P2 P4	P2 P5	P2 P6
	P3	P3 P2	P3 (5%)	P3 P4	P3 P5	P3 P6
	P4	P4 P2	P4 P3	P4 (5%)	P4 P5	P4 P6
	P5	P5 P2	P5 P3	P5 P4	P5 (5%)	P5 P6
	P6	P6 P2	P6 P3	P6 P4	P6 P5	P6 (5%)

Table 4. The operating modes corresponding to various possible two concurrent faults scenarios.

4 depicts details on all the possible configurations for the second bank of filters. For example, if the first fault is detected as a 2% change in the compressor flow capacity (P2), then the first filter in the second level corresponds to the detected fault scenario (P2) (that is $\Delta FC_C = 2\%$), the second filter corresponds to a further decrease of (3%) in the compressor flow capacity resulting in a total of 5% decrease in the capacity (that is $\Delta FC_C = 5\%$), the third filter corresponds to the concurrent decrease of 2% in the compressor flow capacity and a decrease of 2% in the compressor efficiency (P2 and P3) (that is $\Delta FC_C = 2\%$ and $\Delta\eta_C = 2\%$), etc. Note that this procedure can be similarly extended to the third and higher levels that correspond to the occurrence of multiple (three and higher) concurrent faults.

It should be emphasized again that when the new bank of filters is activated in the second level, there is no need to further operate the first bank of filters and our FDI strategy basically deactivates this bank of filters to save computational resources. In other words, the hierarchical architecture enables one to detect and isolate the occurrence of the second fault without adding any extra computational burden since at any given time, only 6 filters are operating on-line.

Remark 3. *Note that in the above hierarchical fault diagnosis architecture, only two levels of fault severities, namely 2% and 5% are considered for the sake of illustration only. It should be emphasized that more fault severities can equally and easily be considered by correspondingly increasing the number of models that are considered in this architecture.*

5 Simulation Results

In this section, simulation results and performance evaluations of our proposed diagnostic system corresponding to various fault scenarios are presented. We have implemented both the EKF and the UKF in our MM-based scheme and have provided comparative results. It should be noted that all the faults are actually applied to and injected in the fully nonlinear model of the jet engine as governed by equations (5) and (6). The measurement noise levels that are considered are shown in Table 5, where the standard deviations are given as percentage of the nominal values at typical cruise conditions [29]. It is also assumed that the PLA=0.9 and the ambient conditions are set to standard conditions and the Mach number is set to 0.74.

N	P_C	T_C	P_T	T_T
0.051	0.164	0.230	0.164	0.097

Table 5. The noise standard deviations (as % of the nominal noise at cruising conditions) [29].

5.1 Single Fault Scenarios

Figures 5 and 6 depict the mode probabilities and the output measurements corresponding to the injected 2% decrease in the compressor efficiency that is applied at $t = 5$ seconds (Mode #3), respectively. In Figure 5 (a), for all $t < 10.2$ seconds the quantity $\arg\max_i p_i(k) = p_1$, which corresponds to classifying and identifying the healthy operation of the engine. However, for all $t >= 10.2$, we have $\arg\max_i p_i(k) = p_3$, which classifies and identifies that the mode $P3$ is active in the engine. Therefore, the fault in the compressor efficiency is perfectly detected and isolated at $t = 10.2$ seconds. As shown in Figure 5, the MM-scheme in which the UKF is used detects the fault at time $t = 10.2$ seconds, whereas the MM-scheme with the EKF detects the fault at time $t = 13.2$ seconds.

Since in real applications there is no guarantee that a fault occurs abruptly or matches exactly the predefined fault severity level, one requires to investigate the performance of the MM-based approach under these realistic circumstances. Figure 7 shows the mode probabilities corresponding to the injection of a 3% fault in the turbine efficiency (Mode #5) corresponding to both the EKF and the UKF detection filters in the MM-based scheme. This figure shows that the algorithm is capable of detecting and isolating a fault whose severity lies within the already designed severities of 2% and 5% and does not have to match the mode definition exactly. The average detection times for all the fault modes (P2 to P6) that are applied at $t = 5$ seconds as a function of the fault severity levels are given in Table 6. Figure 9 shows the detection time as a function of the fault severity for each mode separately. It can be observed from the Table 6 that the higher the fault severity the earlier the detection times specially for faults where the detection filters are specifically designed for.

In next simulation result we evaluate the performance of the fault diagnostic system to a gradually built fault severity level. Specifically, the fault severity is increased from 0 to 3% (the turbine efficiency (Mode #5)) over an interval of 10 seconds.

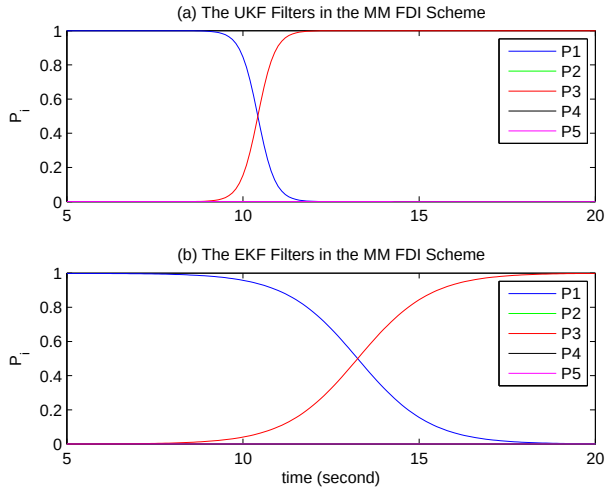

Figure 5. The mode probabilities corresponding to the injected 2% decrease in the compressor efficiency that is applied at $t = 5$ seconds (Mode #3) (a) the UKF is used in the MM-based FDI scheme, and (b) the EKF is used in the MM-based FDI scheme.

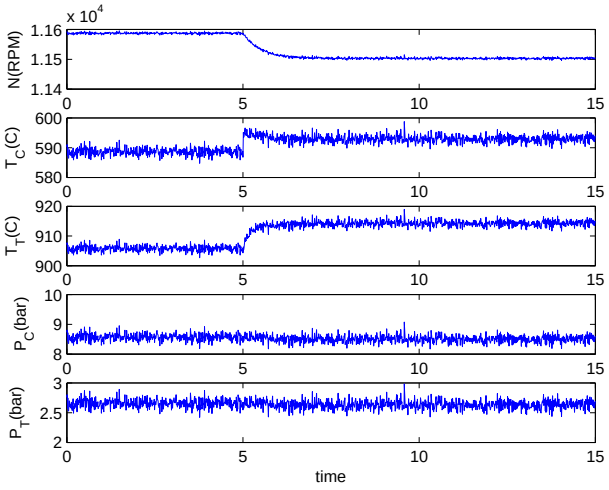

Figure 6. The output measurements corresponding to the injected 2% decrease in the compressor efficiency that is applied at $t = 5$ seconds (Mode #3).

The detection performance of both the EKF and the UKF filters in the MM-based scheme for detecting fault is shown in Figure 8. Although the system is capable of detecting and isolating the fault, however the performance of the diagnostic scheme in terms of detection time is delayed as compared to the case where an abrupt fault is applied (Figure 7). To summarize, as can be observed from the results that are shown in Table 6, the UKF scheme has consistently outperformed the EKF scheme in terms of the delay in the fault detection times.

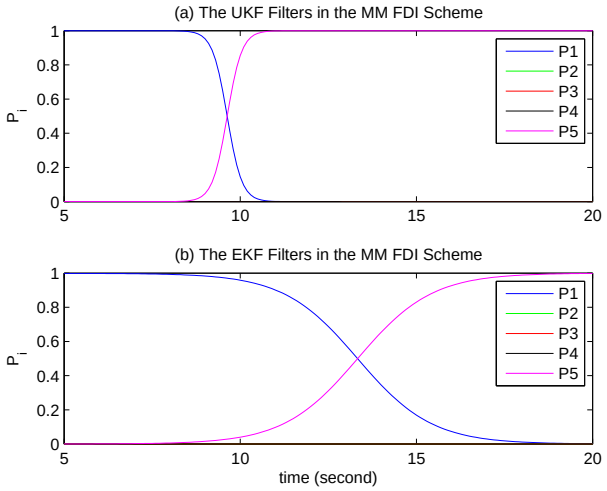

Figure 7. The mode probabilities corresponding to the injected 3% decrease in the turbine efficiency that is applied at $t = 5$ seconds (Mode #5) (a) the UKF is used in the MM-based FDI scheme, and (b) the EKF is used in the MM-based FDI scheme.

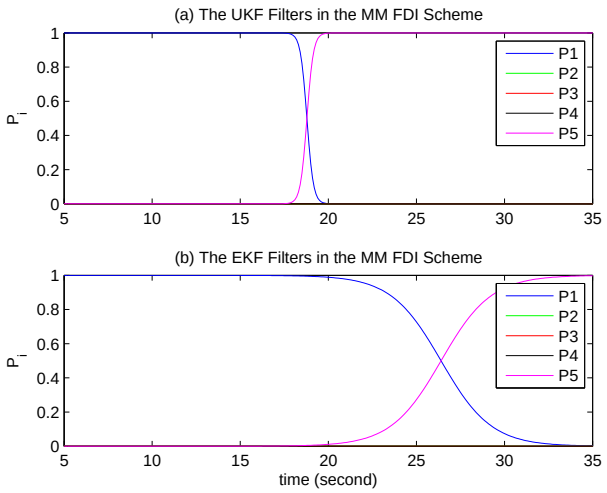

Figure 8. The mode probabilities corresponding to the gradual injection of a 3% decrease in the turbine efficiency that starts at $t = 5$ and linearly ends at $t = 15$ seconds (Mode #5) (a) the UKF is used in the MM-based FDI scheme, and (b) the EKF is used in the MM-based FDI scheme.

5.2 Concurrent Fault Scenarios

In this section, we investigate concurrent faults scenarios where a 2% decrease in the compressor efficiency (P3) is injected at $t = 5$ seconds and a 2% decrease in the compressor mass flow rate (P2) is injected at $t = 30$ seconds. Based on the hierarchical multiple model architecture that was described in Section 4, our proposed algorithm first uses the bank of filters that corresponds to the first level (no fault has yet been detected). Figures 10 (a) and (b) depict the mode probabilities that are generated by the

Fault severity level	2%	3%	4%	5%	6%
UKF Scheme	9.6	10.3	9.5	8.7	9.1
EKF Scheme	11.3	12.9	10.6	10.1	10.4

Table 6. The average detection times for all the fault modes (P2 to P6) that are applied at $t = 5$ seconds as a function of the fault severity levels.

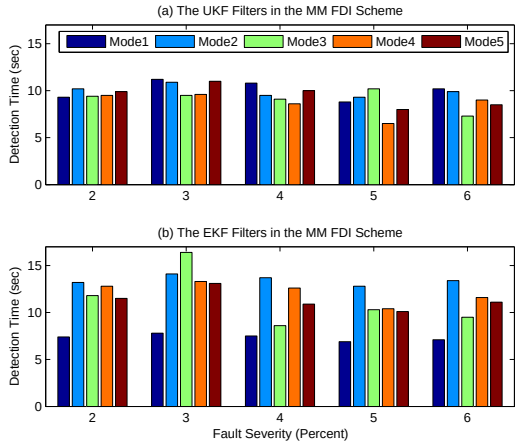

Figure 9. The detection time for each mode of fault that is applied at $t = 5$ seconds as a function of the fault severity (a) the UKF is used in the MM-based FDI scheme, and (b) the EKF is used in the MM-based FDI scheme.

first level filters. As shown in the figures, the first fault in the compressor efficiency is detected and isolated at $t = 10.0$ seconds corresponding to the UKF detection filters and at $t = 12.1$ seconds corresponding to the EKF detection filters.

Once this fault is detected, the second level bank of filters is initiated to operate where these filters are designed according to Table 4. Specifically, the filter #1 in this bank of filters corresponds to the detected fault P3, filter #2 corresponds to the concurrent occurrence of the detected fault P2 and the fault P3, filter #3 corresponds to the further degradation of the compressor efficiency P3 by 3% (resulting in the total decrease of 5%), and similarly for all the other filters they correspond to the concurrent occurrence of the detected fault P2 and the other faults (namely P4 to P6). It should be emphasized again that when a new bank of filters is initiated to run there is no need to further operate the previous level bank of filters so that our proposed FDI algorithm deactivates the previous set of bank of filters. This is done in order to minimize the overall computational resources of the diagnostics system. In other words, at any given time only one set or level of bank of filters is active and running. Figure 10 (c) and (d) depict the mode probabilities that are generated by the second level bank of filters. The second fault in the compressor mass flow rate is detected and isolated at $t = 41.4$ seconds cor-

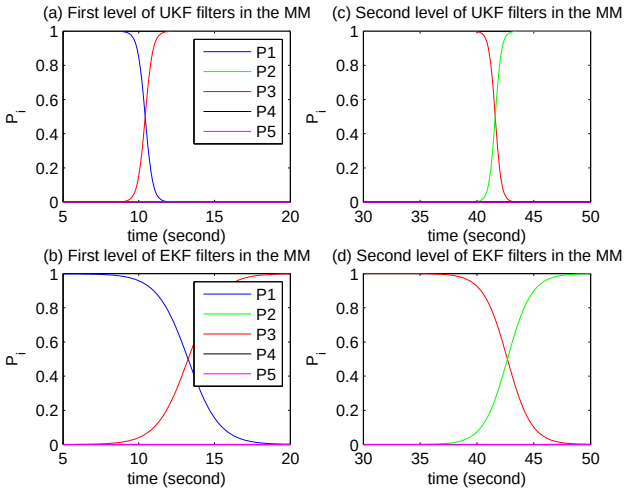

Figure 10. The mode probabilities corresponding to the injected 2% decrease in the compressor efficiency that is applied at $t = 5$ seconds (Mode #3) followed by an injection of a 2% decrease in the compressor mass flow rate (Mode #2 in the second level) that is applied at $t = 30$ seconds. (a) The fault detection and isolation by the first level of filters using the UKF in the MM-based scheme, (b) The fault detection and isolation by the first level of filters using the EKF in the MM-based scheme, (c) The fault detection and isolation by the second level of filters using the UKF in the MM-based scheme, and (d) The fault detection and isolation by the second level of filters using the EKF in the MM-based scheme.

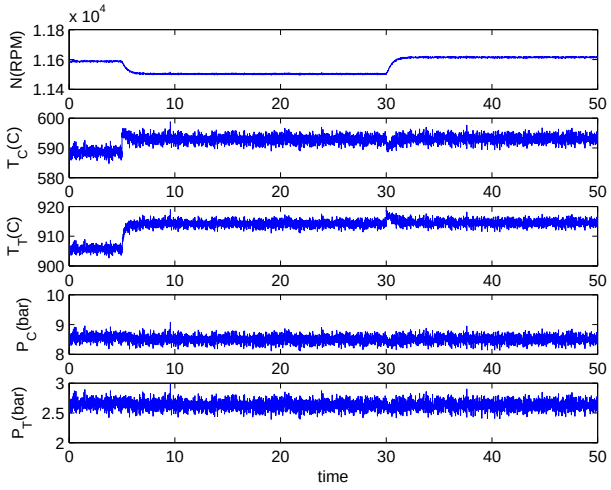

Figure 11. The output measurements corresponding to the injected 2% decrease in the compressor efficiency that is applied at $t = 5$ seconds (Mode #3) followed by an injection of a 2% decrease in the compressor mass flow rate (Mode #2 in the second level) that is applied at $t = 30$ seconds.

responding to the UKF detection filters and at $t = 43.4$ seconds corresponding to the EKF detection filters. As in the previous subsection, one can again conclude that the UKF outperforms the EKF in terms of the delay in the fault detection times. Figure 11 depicts the output measurements that are observed corresponding to the above concurrent faults scenario.

5.3 Operational Condition Variations

When a linear detection filter is used in the MM-based scheme [18], one of the major concerns that arise is due to the validity of the implemented filters subject to the variations of the operating point such as the Mach number, the PLA setting and the ambient conditions. In case of large variations, the diagnostic algorithm may generate false alarms. In order to cope with this drawback, a strategy should be devised to accurately follow the engine operating point variations, and activate the appropriate linear detection filters. However, by implementing our proposed nonlinear detection filters the operating condition variations are automatically taken into account by the nonlinear detection filters. To demonstrate and substantiate this advantage, in the next set of simulations the ambient temperature is linearly varied from from 15° to 5° over an interval of 20 seconds while a 2% fault in the turbine mass flow rate is injected (Mode #4) at time $t = 5$ seconds. Figures 12 and 13 show the results obtained. It follows that while the ambient temperature is varying, the MM-based FDI scheme is capable of detecting and isolating the fault and indeed the operating variations do not affect the FDI performance. In another set of simulations, in addition to the injection of a fault (i.e. a 2% fault in the turbine mass flow rate (Mode #4) applied at $t = 5$ seconds), the PLA is smoothly varied from 0.9 to 1.1, as shown in Figure 15. Our goal here is to investigate the effects of the variation of the Mach number on the performance of the diagnostic scheme. The Mach number is linearly increased from 0.74 to 0.84 in 20 seconds while the fault that is a 2% fault in the turbine mass flow rate (Mode #4) is injected at $t = 5$ seconds. The results of the simulations are shown in Figures 14 and 16 which again confirm and demonstrate the capability of our proposed approach in dealing with the challenging problem of operating condition variations.

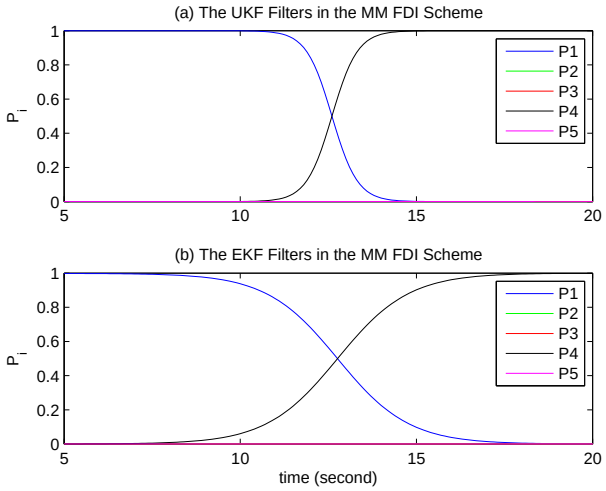

Figure 12. The mode probabilities corresponding to the injected 2% decrease in the turbine mass flow rate that is applied at $t = 5$ seconds (Mode #4) while the ambient temperature is varying (a) the UKF is used in the MM-based FDI scheme, and (b) the EKF is used in the MM-based FDI scheme.

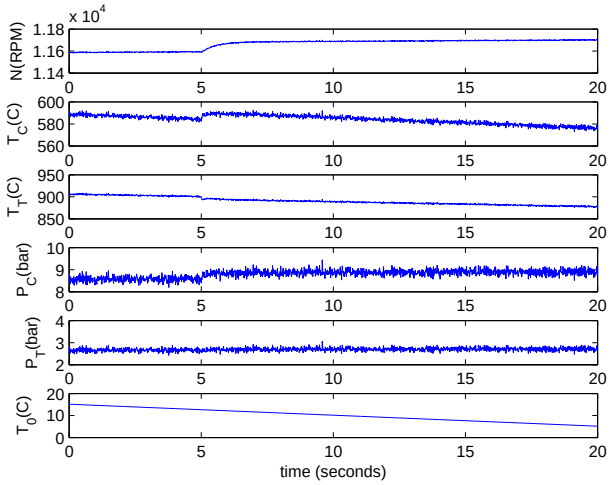

Figure 13. The output measurements corresponding to the injected 2% decrease in the turbine mass flow rate that is applied at $t = 5$ seconds (Mode #4) while the ambient temperature is varying.

5.4 A Comparison Between the Performance of the UKF and the EKF Detection Filters

In this section, we investigate the performance of the the UKF and the EKF detection filters in the MM-based scheme. An important figure of merit that is of interest in many applications is robustness to sensor and measurement noise. In the previous simulations, we have applied a noise level that is given in Table 5 for the measurements. In this subsection, we have increased the noise levels proportionally by a factor (noise power factor), and have examined if the UKF or the EKF detection filters in the MM-based scheme are capable of detecting and isolating all fault modes as described in Table 3. The detection time for each fault mode as a function of the noise power factor is shown in Figure 17. The results are summarized in Table 7 in which numerical values indicate the average fault detection times for all the modes (P2 to P6) when the fault is applied at $t = 5$ seconds. A bullet mark ($\bullet$) indicates an unsuccessful detection or isolation of at least one fault mode. As expected, the UKF scheme demonstrates a superior performance over the EKF scheme when a higher level of noise is applied.

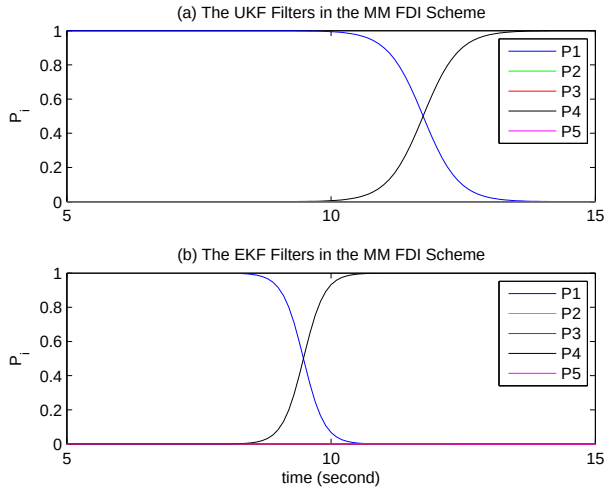

Figure 14. The mode probabilities corresponding to the injected 2% decrease in the turbine mass flow rate that is applied at $t = 5$ seconds (Mode #4) while the PLA is varying (a) the UKF is used in the MM-based FDI scheme, and (b) the EKF is used in the MM-based FDI scheme.

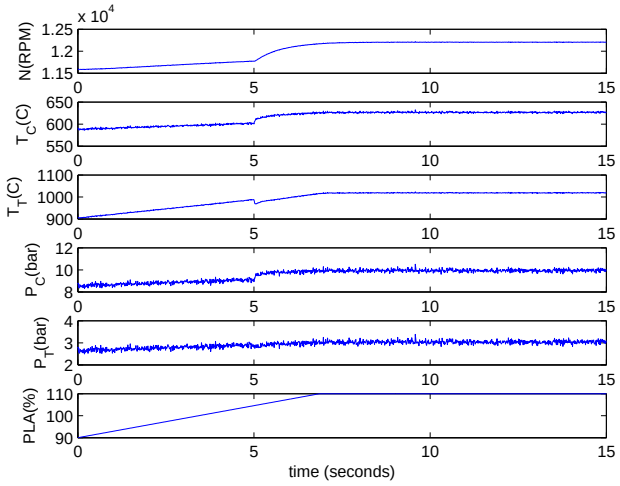

Figure 15. The output measurements corresponding to the injected 2% decrease in the turbine mass flow rate that is applied at $t = 5$ seconds (Mode #4) while the PLA is varying.

In another set of simulations, we have investigated the effects of the availability of a certain number of measurements on the performance of the detection filters. This case is different from the sensor fault scenario since in the presence of a sensor fault the diagnostic or control module will continue to use the faulty sensor data unless a separate strategy for sensor fault detection is employed and considered. In this subsection, we are interested in determining the minimum number of measurements that is required by the detection filters in order to perform the

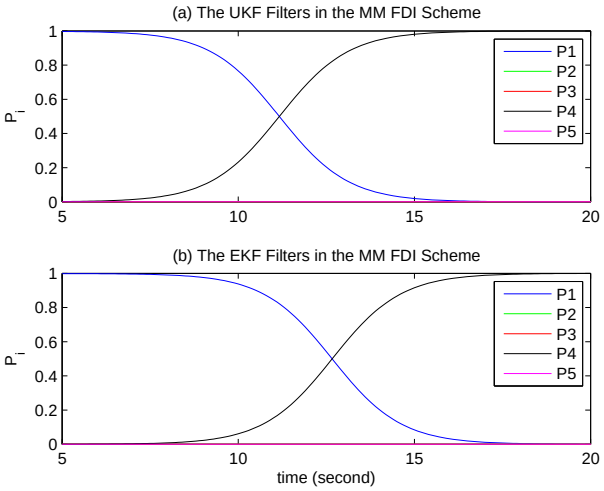

Figure 16. The mode probabilities corresponding to the injected 2% decrease in the turbine mass flow rate that is applied at $t = 5$ seconds (Mode #4) while the Mach number is varying (a) the UKF is used in the MM-based FDI scheme, and (b) the EKF is used in the MM-based FDI scheme.

Noise power factor	1	1.1	1.3	1.5	1.8	2
UKF Scheme	9.6	9.8	10.0	9.9	10.1	10.1
EKF Scheme	11.3	15.6	19.2	•	•	•

Table 7. The average detection times for all the modes of faults (P2 to P6) that are applied at $t = 5$ seconds as a function of the noise power factor.

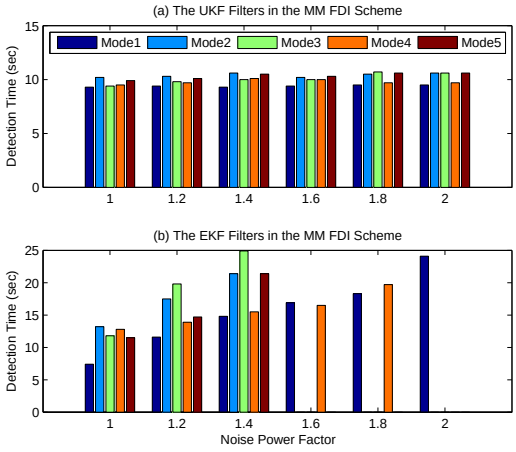

Figure 17. The detection time for each mode of fault that is applied at $t = 5$ seconds as a function of the noise power factor. The empty places indicates the unsuccessful detection or isolation of the corresponding fault. (a) the UKF is used in the MM-based FDI scheme, and (b) the EKF is used in the MM-based FDI scheme.

Number of measurements/sensors used	5	4	3	2
UKF Scheme	9.6	11.7	12.0	•
EKF Scheme	11.3	13.5	14.1	•

Table 8. The average detection times for all the fault modes (P2 to P6) that are applied at $t = 5$ seconds as a function of the number of the measurements or sensors that are employed.

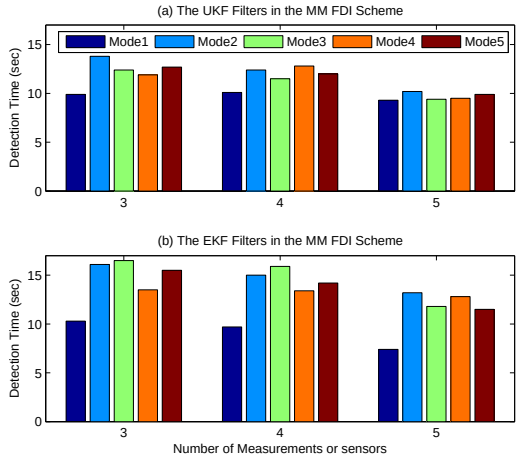

Figure 18. The detection time for each mode of fault that is applied at $t = 5$ seconds as a function of the number of the measurements or sensors that are employed. (a) the UKF is used in the MM-based FDI scheme, and (b) the EKF is used in the MM-based FDI scheme.

FDI task properly. The detection time for each fault mode as a function of the number of the measurements or sensors is shown in Figure 18. Table 8 summarizes the results. In this table the average fault detection times numerical values for all the modes (P2 to P6) are provided corresponding to a fault that is applied at $t = 5$ seconds. A bullet mark (•) indicates either an unsuccessful detection or isolation of at least one fault mode. It can be concluded that both the UKF and the EKF detection filters have the same performance capability in terms of functionality with various sets of measurements and sensors, however, the UKF detection filters perform superior over the EKF detection filters in terms of the fault detection times.

Computational requirements is also an important merit of performance which one requires to consider for comparison and evaluation purposes. The UKF scheme in general runs slower than the EKF scheme due to the multiple nonlinear computations that are required at each time step. This factor makes the UKF scheme less suitable for real-time applications. On the other hand, one of the advantages of the UKF scheme over the EKF scheme is that it does not require the Jacobian matrix of the system at each time step, which by itself is a computationally costly operation. Especially, when one uses performance maps for modeling the nonlinear dynamics of the jet engine, the task of computing the Jacobian matrix at each operating point is computationally expensive and complex and can be performed only numerically. However, in our application the linearization approximation performed by the EKF scheme at each time step takes less CPU time than the multiple nonlinear computations that are performed by the UKF scheme.

Based on the above simulations and discussions, it can be concluded in the final analysis that the UKF detection filters do indeed outperform the EKF detection filters in this application.

6 Conclusions

In this paper, a nonlinear multiple model (MM-based) fault detection and isolation scheme for health monitoring of jet engines is proposed and developed. Starting from the nonlinear dynamics of a jet engine, a bank of nonlinear detection filters is designed where each filter corresponds to a specific faulty mode of the engine. A hierarchical fault detection and isolation architecture is proposed corresponding to both single and concurrent faults in the engine. By taking into account the fault occurrence history, only a minimal set of detection and isolation filters is activated so that the same number of filters are always operating at any given point in time. In other words, the complexity of our proposed fault detection and isolation (FDI) algorithm does not increase as more novel faults are concurrently injected to the engine. We have implemented both the EKF and the UKF detection filters in the MM-based FDI architectures. Simulation results demonstrate that considerable improvements exist on the performance of the UKF scheme over the EKF scheme in terms of the fault detection times and functionality with respect to different number of measurements and sensors. Moreover, the UKF scheme is significantly more robust to the large sensor noise. In this work, we have assumed existence of a set of predefined severity fault levels for construction of the supposed UKF and EKF detection filters from the corresponding nonlinear model of the jet engine. Therefore, one natural direction for future research will be to develop a robust fault diagnosis scheme in which the fault severity levels are estimated through parameter estimation techniques.

REFERENCES

[1] J. Gertler, "Model based fault daignosis," *control theory and advanced technology*, vol. 9, no. 1, pp. 259–285, 1993.

[2] P. M. Frank, "fault diagnosis in dynamics systems using analytical and knowledge-based redundancy- a survey," *Automatica*, vol. 26, no. 3, pp. 459–474, 1990.

[3] P. Maybeck, "Multiple model adaptive algorithms for detecting and compensating sensor and actuator/surface failures in aircraft flight control systems," *International Jour-*

nal of Robust and Nonlinear Control, vol. 9, pp. 1051–1070, 1999.

[4] T. Menke and P. Maybeck, "Sensor/actuator faiiure detection in the vista f-i6 by multiple model adaptive estimation," *IEEE Transactions on Aerospace and Electronic Systems*, vol. 31, no. 4, pp. 1218–1229, 1995.

[5] Y. Zhang and J. Jiang, "An interacting multiple-model based fault detection, diagnosis fault-tolerant control approach," *Proceedings of the 38th Conference on Decision and Control, Phoenix, Arizona USA*, pp. 3593–3598, 1999.

[6] G. G. Yen and L. Ho, "Online multiple-model-based fault diagnosis and accommodation," *IEEE Transactions On Industerial Electronics*, vol. 50, no. 2, pp. 296–312, 2003.

[7] R. J. Patton, C. J. L. Toribiot, and S. Simanit, "Robust fault diagnosis in a chemical process using multiple-model approach," *Proceeding of the 40th IEEE Conference on Decision and Control,Orlando, Florida USA*, pp. 149–154, 2001.

[8] E. A. Garcia and P. M. Frank, "Deterministic nonlinear observer-based approaches to fault diagnosis: A survey," *Control Engineering Practice*, vol. 5, no. 5, pp. 663–670, 1997.

[9] C. Depersis and A. Isidori, "A geometirc approach to nonlinear fault detection and isolation," *IEEE Transaction on Automatic Control*, vol. 46, no. 6, pp. 853–865, 2001.

[10] A. Xu and Q. Zhang, "Nonlinear system fault diagnosis based on adaptive estimation," *Automatica*, vol. 40, pp. 1181–1193, 2004.

[11] R. J. Patton and J. Chen, "Robust fault detection of jet engine sensor systems using eigenstructure assignment," *Journal of Guidance, Control and Dynamic*, vol. 15, no. 6, pp. 1491–1497, 1992.

[12] ——, "Modelling methods for improving robustness in fault diagnosis of jet engine system," *In Proceeding of the 31st IEEE Conference on Control and Decision, Tucson, Arizona*, pp. 2330–2335, 1997.

[13] L. A. Urban, "Gas path analysis applied to turbine engine conditioning monitoring," *AIAA/SAE*, 1972, paper 72-1082.

[14] A. J. Volponi, "Foundations of gas path analysis," in *Gas Turbine Condition Montiring and Fault Diagnosis*, C. H. . Sieverding and K. Mathioudakis, Eds. Belgium: von Karman Isntitute, 2003.

[15] W. C. Merrill, J. C. DeLaat, and W. M. Bruton, "Advanced detection, isolation, and accommodation of sensor failures:real-time evaluation," *Journal of Guidance, Control, and Dynamics*, vol. 11, pp. 517–526, 1988.

[16] T. Kobayashi and D. L. Simon, "Application of a bank of kalman filters for aircraft engine fault diagnostics," *Turbo Expo*, 2003, GT 2003-38550.

[17] D. Simon, "A comparison of filtering approaches for aircraft engine health estimation," *Aerospace Science and Technology*, vol. 12, no. 4, pp. 276–284, 2008.

[18] N. Meskin, E. Naderi, and K. Khorasani, "Fault diagnosis of jet engines by using a multiple model based approach," *ASME Turbo Expo Conference*, GT 2010-23442.

[19] J. Kurzke, "How to get component maps for aircraft gas turbine performance calculations," *International Gas Turbine and Aeroengine Congress and Exposition*, 1996.

[20] ——, "Advanced user-friendly gas turbine performance calculation on a personal computer," *International Gas Turbine and Aeroengine Congress and Exposition*, 1995.

[21] W. P. J. Visser and M. J. Broomhead, "GSP, a generic object-oriented gas turbine simulation environment," *International Gas Turbine and Aeroengine Congress and Exposition*, 2000.

[22] E. A. Wan and R. V. D. Merwe, "The unscented kalman filter for nonlinear estimation," *Adaptive Systems for Signal Processing, Communications, and Control Symposium*, pp. 153 – 158, 2000.

[23] P. Eide and P. Maybeck, "An MMAE failure detection system for the F-16," *IEEE Transactions on Aerospace and Electronic Systems*, vol. 32, no. 3, pp. 1125–1136, 1996.

[24] S. M. Camporeale, B. Fortunato, and M. Mastrovito, "A modular code for real time dynamic simulation of gas turbines in SIMULINK," *Journal of Engineering for Gas Turbines and Power*, vol. 128, pp. 506–517, 2006.

[25] V. Panov, "GASTURBOLIB-SIMULINK library for gas turbine engine modelling," *Proceedings of ASME Turbo Expo: Power for Land, Sea and Air*, 2000.

[26] G. L. Merrington, "Fault diagnosis in gas turbines using a model-based technique," *Journal of Engineering for Gas Turbines and Power*, vol. 116, no. 2, pp. 374–380, 1994.

[27] R. Mohammadi, E. Naderi, K. Khorasani, and S. Hashtrudi-Zad, "Fault diagnosis of gas turbine engines by using dynamic neural networks," *ASME Turbo Expo Conference*, GT2010-23586.

[28] A. J. Volponi, "Extending gas path analysis coverage for other fault conditions," in *Gas Turbine Condition Montiring and Fault Diagnosis*, C. H. . Sieverding and K. Mathioudakis, Eds. Belgium: von Karman Isntitute, 2003.

[29] K. Mathioudakis, C. Romessis, and A. Stamatis, "Probabilistic methods for gas turbine fault diagnostics," in *Gas Turbine Condition Montiring and Fault Diagnosis*, C. H. . Sieverding and K. Mathioudakis, Eds. Belgium: von Karman Isntitute, 2003.